THE JOURNAL OF PHYSICAL CHEMISTRY Letters

Letter

pubs.acs.org/JPCL

Nanoscale Internal Fields in a Biased Graphene–Insulator–Semiconductor Structure

Sylvie Rangan,*[,†,‡] Malathi Kalyanikar,[§] Junxi Duan,[†] Gang Liu,[∥] Robert Allen Bartynski,[†,‡] Eva Y. Andrei,[†] Leonard Feldman,[∥] and Eric Garfunkel[§,∥]

[†]Department of Physics and Astronomy and [‡]Laboratory for Surface Modification, Rutgers University, 136 Frelinghuysen Road, Piscataway, New Jersey 08854, United States

[§]Department of Chemistry and Chemical Biology, Rutgers University, 610 Taylor Road, Piscataway, New Jersey 08854, United States

[∥]Institute for Advanced Materials, Devices and Nanotechnology, Rutgers University, 607 Taylor Road, Piscataway, New Jersey 08854, United States

Supporting Information

ABSTRACT: Measuring and understanding electric fields in multilayered materials at the nanoscale remains a challenging problem impeding the development of novel devices. At this scale, it is far from obvious that materials can be accurately described by their intrinsic bulk properties, and considerations of the interfaces between layered materials become unavoidable for a complete description of the system's electronic properties. Here, a general approach to the direct measurement of nanoscale internal fields is proposed. Small spot X-ray photoemission was performed on a biased graphene/SiO_2/Si structure in order to experimentally determine the potential profile across the system, including discontinuities at the interfaces. Core levels provide a measure of the local potential and are used to reconstruct the potential profile as a function of the depth through the stack. It is found that each interface plays a critical role in establishing the potential across the dielectric, and the origin of the potential discontinuities at each interface is discussed.

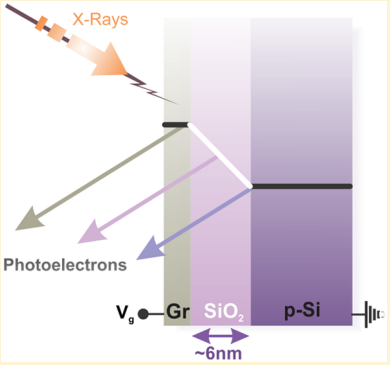

Understanding how the electrostatic potential varies across a multilayered thin-film system is central to the development of novel micro- and nanoelectronic technologies. The interfacial energy band alignment, as well as how the local potential varies in the different layers in the presence of an external voltage placed across a given structure, dictates some key device properties. Furthermore, the electrostatic potential within a multilayer structure may become particularly complex when defects, either interfacial or embedded within films, fixed or mobile, neutral or charged, must be considered. The use of two-dimensional (2D) materials such as graphene or transition-metal dichalcogenides, whose properties can be tuned from metallic to semiconducting, adds another level of complexity yet offers additional control of devices' capabilities. Understanding the nature of the interfaces of 2D materials with dielectrics is thus central to controlling the response of a device to an electric field.

Studies of ultrathin dielectrics on semiconductors are routinely performed using surface sensitive techniques such as X-ray photoelectron spectroscopy (XPS), and several studies have monitored XPS line shapes while modifying the surface potential. Several decades ago, Lau et al. developed a form of XPS-based surface charge spectroscopy performed on several oxide/semiconductor systems.[1] By exposing the dielectric surface to a constant flow of either electrons or X-rays, both positive and negative charging of a dielectric grown on a semiconductor were achieved. The experimentally determined photoemission intensities, including broadening and peak shifts, were modeled by making some basic assumptions regarding semiconductor band bending, potential profile across the oxide, and possible defects states in the film.[1−6] Cohen and co-workers have extended the application of flood gun charging strategies to a wider class of interfaces using the phrase "chemically resolved electrical measurements" to describe their method.[7−10] Suzer et al. have performed extensive XPS-based measurements on defects and charging effects in oxides[11−16] and have also recently explored in-plane surface potential variations using XPS imaging on in-plane biased structures.[17−19] Lastly, Kobayashi et al., have applied a bias across a metal/oxide/semiconductor (MOS) stack using 3 nm Pt films as top electrodes and performed XPS in order to model the oxide defects density based on the evolution of the substrate band bending.[20−22] In all these studies, however, the determination of the potential profile across an entire stack was never performed.

In this Letter, a new small spot XPS-based method to probe the electrostatic potential profile across a biased multilayer system is demonstrated. The approach consists of performing XPS measurements of a graphene–oxide–semiconductor

Received: August 10, 2016
Accepted: August 17, 2016

DOI: 10.1021/acs.jpclett.6b01806
J. Phys. Chem. Lett. 2016, 7, 3434−3439

structure composed of a highly doped Si substrate, a 60 Å thermally grown SiO_2 oxide, and a graphene (Gr) overlayer, as shown in Figure 1. The measurements have been performed

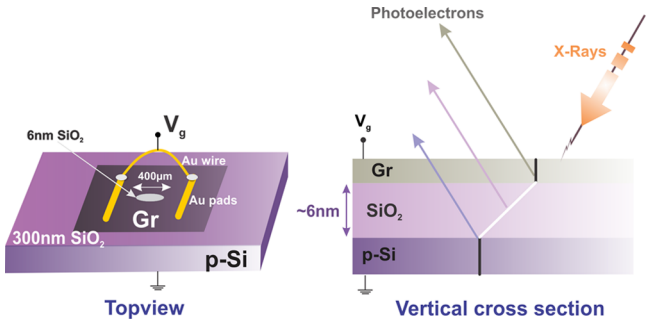

Figure 1. Graphene−SiO_2−Si stack biased during X-ray photoemission experiments. The graphene top electrode ensures that a uniform and readily quantifiable potential is applied to the surface, while enabling photoelectrons emitted from the SiO_2 and Si substrate to be detected.

with the Si substrate grounded and the graphene gate held at a series of applied potentials between −2.7 and +2.7 V. Because of the short mean free path of the photoemitted electrons, the combined thickness of the graphene and the oxide has been chosen to be less than 8 nm, so that core level features from all components of the system, including the first layers of the substrate, contribute to the observed XPS spectrum. By measuring and then modeling changes in the core level line shapes as a function of bias, we can establish a profile of the electrostatic potential across the system.

The system under study can be considered as a simple MOS capacitor stack with the overlayer, a chemical vapor deposition (CVD)-grown graphene, acting as an ultrathin metallic electrode. The conventional representation of potential profiles across MOS stacks under different bias conditions is summarized in Figure 2.

In this representation, the degenerately doped (10^{19} cm^{-3}) p-Si base is kept at ground potential and a bias V_g is applied to the metallic gate (graphene). Because most MOS stacks are not ideal, a small bias (the flatband voltage V_{fb}) is required to move the system into a flatband condition, as shown in Figure 2. At flatband voltage there should ideally be no potential drop across the oxide layer and no band bending in the silicon. With a decrease in the gate voltage ($V_g < V_{fb}$), the system shifts to an accumulation regime where the majority carriers (holes from Si) are attracted toward the negative electrode. The application of a bias attracts the majority carriers in this highly doped system to an extent such that most of the potential drop is expected to occur in the oxide layer. For $V_g > V_{fb}$, the reverse trend is seen, with the movement of the majority carriers away from the direction of bias (the depletion regime). Here the potential drop may be observed across both the oxide and the silicon substrate in the form of band bending, as there are few carriers in the Si when biased in the depletion regime.

In this biased photoemission experiment, the system can be viewed as a single layer of carbon atop a SiO_2 film, which can be treated as a series of parallel slabs, over a single layer of elemental Si. In this "slab model", the total oxide thickness, t, is divided into a series of n slabs of equal thickness ($d = t/n$), parallel to the surface. Each slab contributes to the total photoemission peak, $I(E)$, by its intensity $I_n(E)$, such that

$$I(E) = \sum_n I_n(E) = \sum_n I_0(E + \Delta_n)e^{-nd/\lambda} \quad (1)$$

where $I_0(E)$ is the photoemission peak intensity originating from the topmost slab, Δ_n the energy shift caused by the local potential in a given slab (Δ_n is negative for negative bias and positive for the positive bias), d the thickness of a slab, and λ the attenuation length of photoelectrons in the oxide layer. In such a model, the total photoemission contribution from the oxide is obtained as the sum of I_n over the thickness of the oxide. Therefore, it is expected that applying a bias across the oxide should both shift and broaden the photoemission peak without altering the total area under the peak.

To determine $I_0(E)$, one must obtain the shape and position of the oxide photoemission peaks, unperturbed by the presence of potential variations across the oxide layer. This situation corresponds to the flatband condition and is experimentally determined for our system at $V_g = -0.6$ eV, when the smallest full width at half-maximum for the oxide peaks is obtained.[23,24] For comparison, using an electron affinity for silicon of 4.1 V,[25] a graphene workfunction of 4.56 V,[26] and our doping level of 10^{19} cm^{-3}, a flatband voltage of −0.64 V is predicted using the calculation scheme applicable to nondegenerate silicon substrates.

A central requirement for this experiment is the ability to apply a uniform and well-defined bias across the Gr/SiO_2/Si stack. Because the Gr electrode is the dominant source of carbon in the system, the effective bias can be measured by following the C 1s levels, as shown in Figure 3a. At the flatband voltage, i.e., when a −0.6 V is applied to the graphene electrode, the maximum of the carbon peak is found at a binding energy of 284.1 eV. When biases of −2.7 and +2.7 V are applied, the C 1s peak rigidly shifts by 2.0 eV toward lower binding energies and 3.3 eV toward higher binding energies, respectively, as expected. Therefore, monitoring the carbon peak position is a viable and accurate (within our error bars) method to determine the top electrode potential, and agrees well with the externally applied voltage. We also note that biasing does

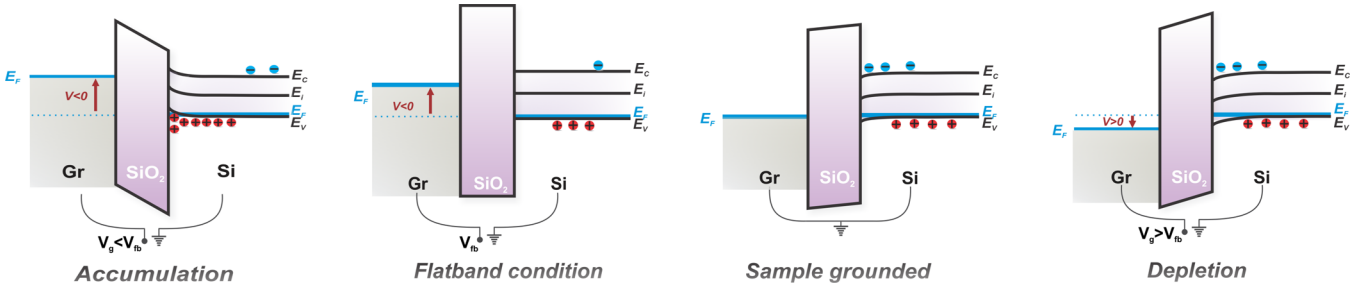

Figure 2. Different bias regimes and their corresponding band energy diagrams.

DOI: 10.1021/acs.jpclett.6b01806
J. Phys. Chem. Lett. 2016, 7, 3434−3439

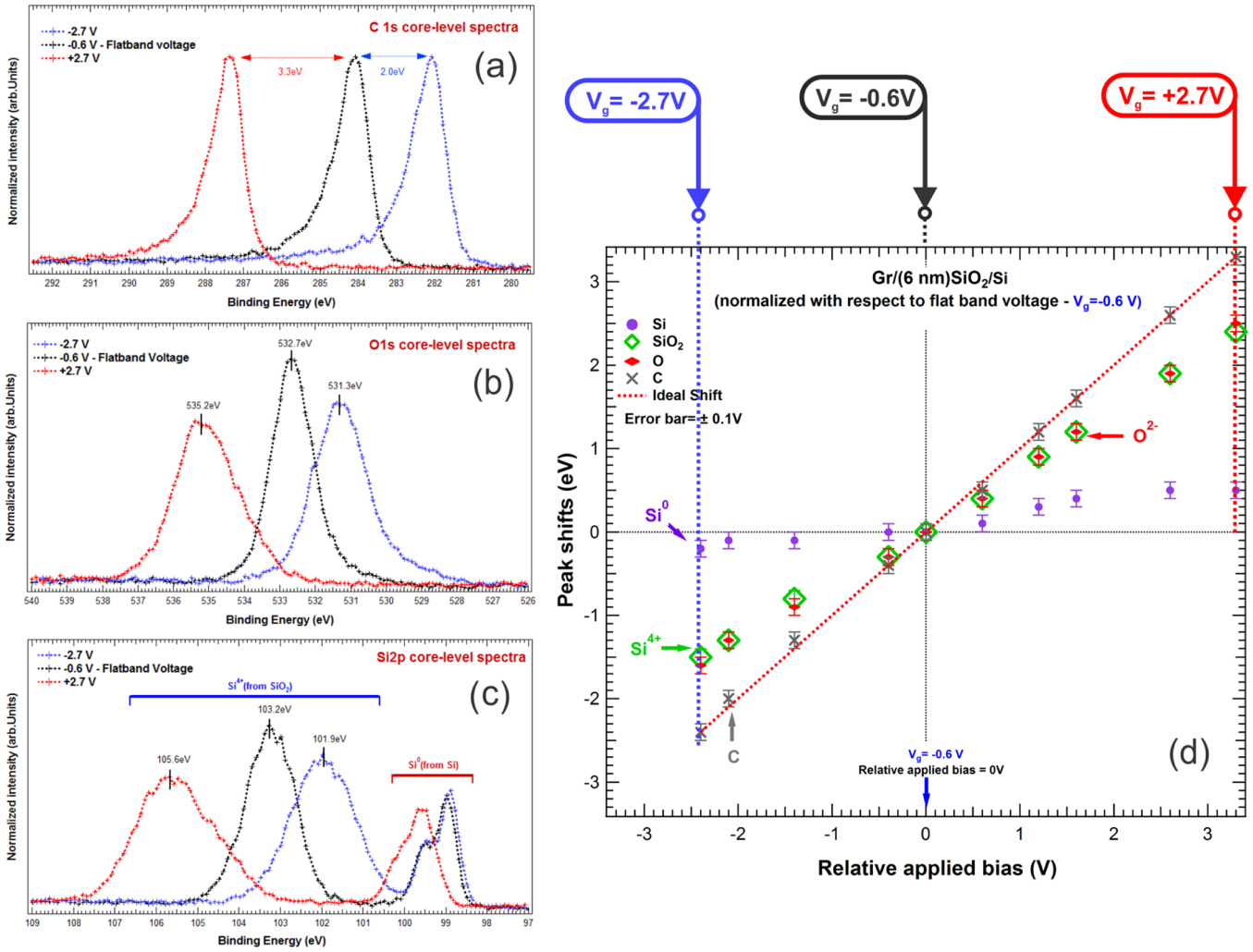

Figure 3. Core level spectra measured for three biasing conditions (−2.7 V, −0.6 V, and +2.7 V): (a) C 1s core-level, (b) O 1s core-level, and (c) Si 2p core-level. (d) Summary of the peak maxima shifts measured as a function of the relative applied bias (with respect to flatband condition set at 0 V).

not alter the shape of the C 1s peak, indicating that the entire top electrode (which may contain some carbon other than graphene such as residual polymer or adventitious carbon) is an equipotential surface.

The situation is more complex when analyzing the O 1s core level. Although most of the O is located in the SiO_2 layer, a small component (<5%) of the oxygen peak can be attributed to adsorbed species at the surface of either the SiO_2 layer or the top Gr electrode. At flatband, the O 1s peak is nearly symmetric and centered around 532.7 eV, as shown in Figure 3b. When a −2.7 V bias is applied, the O 1s peak broadens and changes shape, and the position of the most intense part of the peak shifts approximately 1.4 eV toward lower binding energies. When a +2.7 V bias is applied, the O 1s peak broadens in the other direction and shifts 2.5 eV toward higher binding energies. Here the observed shifts are not equal to the bias difference seen by the top Gr electrode, as the final peak position is the result of a weighted sum of O 1s peaks at different positions in the film, each with its own local potential, less than that of the graphene electrode. Nevertheless, the integrated area under each O 1s peak is constant, as expected based on eq 1.

The behavior of the Si 2p core level peak region is shown in Figure 3c. The Si 2p core level spectra contain information pertaining to both the oxide (Si^{4+} oxidation state) and the silicon substrate (Si^0 oxidation state) and indicate no visible contribution from suboxides at the interface.[27] At flatband voltage, the Si $2p_{3/2}$ components for the oxide and for the bulk silicon are found at 103.2 and 98.9 eV, respectively. Here, the oxide-related Si peaks clearly follow the qualitative trends observed for the O 1s oxide peak as a function of applied bias. The Si^0 peak is also modified upon biasing, although to a much less extent, as it is electrically held closer to the grounded side of the sample. A small 0.1 eV shift toward lower binding energies is measured upon application of a −2.7 V bias, while a larger 0.6 eV shift toward higher binding energies is measured when applying +2.7 V, concurrent with visible broadening.

Similar sets of XPS spectra have been acquired for different biasing conditions (see Supporting Information). A summary of the core level peak maxima shifts is reported in Figure 3d using a scale referenced to the flatband voltage. The Gr behaves as a metallic electrode, shifting exactly as it should within experimental error. Additionally, both the oxide O 1s and Si 2p core levels also shift, although to a lesser extent, as discussed above. Finally, the substrate Si 2p peak does shift, although

DOI: 10.1021/acs.jpclett.6b01806
J. Phys. Chem. Lett. 2016, 7, 3434−3439

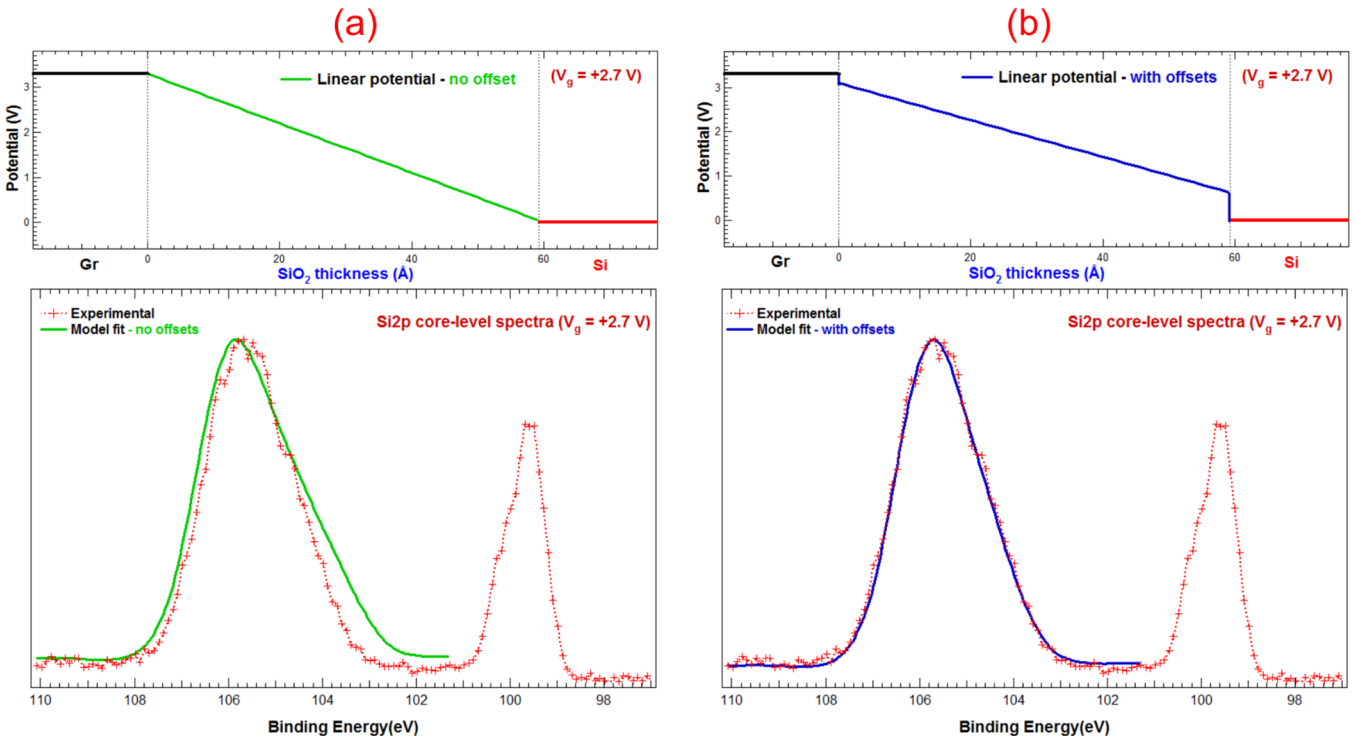

Figure 4. Models for the potential profile determination across the Gr−SiO_2−Si structure. (a) A model with a simple linear potential profile in the dielectric does not result in a convincing simulation of the experimental biased-XPS data. (b) When potential offsets at each interface are added to a linear potential drop across the dielectric, the simulated spectrum follows the biased-XPS data quite accurately.

much less than the other peaks, indicating band bending in the Si substrate.

These results can be qualitatively understood in the framework of conventional MOS capacitor behavior, Figure 2. Using the flatband condition ($V_g = V_{fb} = -0.6$ V) as a reference point, one can understand the MOS potential profile when in the accumulation ($V_g < V_{fb}$) and depletion ($V_g > V_{fb}$) regimes. (Note that the inversion regime is typically attained only for larger applied biases for such samples.) In particular, we observe that the band bending in the silicon substrate is more prominent in the depletion regime, a result of the larger energy swing possible in the gap while in depletion before inversion essentially fixes the maximum potential swing. At its maximum (which occurs before 2.7 V), a shift of about 0.6 eV toward higher binding energies is measured for the Si^0 component of the Si 2p core level, and a broadening of the photoemission peak is observed. This broadening, although typically not observed for medium-doped Si substrates, is due to the high doping level of our substrate, therefore leading to a severe narrowing of the depletion width in the silicon substrate.[28−30] The extent and magnitude of the band bending into the silicon substrate for both positive and negative biases are comparable to recent experimental and theoretical studies of band bending measured using scanning tunnel microscopy and spectroscopy.[31,32]

In order to extract the potential profile across the MOS structure from our photoemission data set, a more quantitative analysis is needed. As a first approximation, we assume that the potential profile in the high-quality thermal SiO_2 between the two electrodes, Gr and Si, is perfectly linear, as represented in the top part of Figure 4a. Using eq 1, and using the Si 2p photoemission peak at flatband condition as reference, a simulated spectrum for the Si 2p line shape from the SiO_2 film generated by summing all I_n contributions over the SiO_2 thickness with a slab thickness of 1 Å is shown at the bottom of Figure 4a, superimposed over our experimental data obtained for an applied bias of +2.7 V. Although the general trends are correct, there are clear discrepancies between this model and the experimental spectra. We then explored a refined model which permits potential discontinuities at both interfaces, as illustrated in the top part of Figure 4b. The potential discontinuities, in essence, are dipoles located at the interfaces, which can be determined via a χ^2 fitting procedure of our experimental data. An example of such a model spectrum for the Si 2p peak of the oxide is shown in the bottom part of Figure 4b. Under these simple assumptions, the result of the fit is remarkably good.

Using the same assumptions, the potential offsets at both interfaces have been calculated for different applied V_g and are reported in Table 1. Additionally, the measured Si $2p_{3/2}$ peak shift of Si^0 is reported as a reference for the relative amount of band bending in Si, as a function of V_g.

The first noticeable characteristic of the offsets is that they are not constant as a function of the applied bias. In the case of the SiO_2−Si interface, this can be easily understood by realizing that the calculated offset closely follows the experimentally measured Si substrate peak shift of Table 1. This indicates that the potential drop at this interface is directly related to the band bending in the substrate.

The situation is more complex at the Gr−SiO_2 interface. Because both the relative intensity and the direction of the offset follow the applied bias, it is possible that something forming a dipole at the Gr−SiO_2 interface could be responsible for such behavior. Recent studies suggest the presence of water at the Gr−SiO_2 interface for preparation conditions similar to ours,[33] where either CVD-grown graphene is deposited onto

DOI: 10.1021/acs.jpclett.6b01806
J. Phys. Chem. Lett. 2016, 7, 3434−3439

Table 1. Gate Bias (V_g), Calculated Bias Offsets at the Gr−SiO_2 and SiO_2−Si Interfaces, and Measured Shift of the Silicon Substrate Si $2p_{3/2}$ Peak

V_g	Gr−SiO_2 offset	SiO_2−Si offset	measured Si^0 peak shift
−3.0	−0.3	−0.3	−0.2
−2.7	−0.3	−0.2	−0.1
−2.0	−0.2	−0.1	−0.1
−1.0	0.0	0.0	0.0
−0.6	0.0	0.0	0.0
0.0	0.0	0.0	+0.1
+0.6	+0.1	+0.4	+0.3
+1.0	+0.1	+0.4	+0.4
+1.5	+0.2	+0.6	+0.5
+2.0	+0.1	+0.6	+0.5
+2.7	+0.2	+0.6	+0.5

SiO_2 in atmospheric conditions using solution-based process or where graphene is prepared via exfoliation.[34−36] Although annealing can help remove interface adsorbates, some may still remain trapped at the interface. If the impurity species is polar or very polarizable, it can contribute significantly to an interface offset.[34] To establish a scale for the value of such interface dipole, we can consider the extreme case of a surface fully covered with water molecules in which the dipoles are all aligned perpendicularly to the surface plane. Considering for water a dipole D = 1.84 D and a molecular diameter $\delta \sim 3$ Å, the interface dipole can be estimated from a planar capacitor formula as $\Delta V = D/\epsilon_0 \times A$, where A is the footprint of a molecule ($A = \pi(\delta/2)^2$) and ϵ_0 is the vacuum permittivity, to be 9.8 V. This is obviously an unrealistic value because the water coverage may be smaller and the dipoles will likely not all orient favorably, but this gives some credibility to the role of polar adsorbates as one explanation for interface dipoles of the order of 0.3 eV. This suggests that larger biases would tend to orient a larger number of adsorbates, creating a dipole in the direction opposite to the applied bias.

In summary, we have demonstrated that using a novel experimental configuration to create a biased graphene/SiO_2/Si stack, we are able to employ small spot X-ray photoelectron spectroscopy not only to retrieve the potential profile across the dielectric layer but also to characterize and quantify the response of the entire stack to an electric field. Using this approach, we can accurately and controllably apply a potential across the stack. A detailed analysis of the shape and energy of the C 1s, O 1s, and Si 2p core level spectra indicates that a simple linear potential profile across the nanoscale high-quality SiO_2 can reproduce the experimental data, but more importantly that each interface plays a critical role in establishing the potential across the dielectric. At the SiO_2/Si interface, a potential drop is measured and related to band bending into the semiconductor, and at the graphene/SiO_2 interface, a potential discontinuity could possibly be related to polarizable species (such as trapped water or other species) opposing the applied electric field. Because there is no intrinsic limitation inherent to this technique, sample preparation challenges aside, this unique experimental approach offers new possibilities for addressing problems that have until now prevented further scaling of devices and 2D material integration. Biasing effects on other dielectric thin films, and using 2D layered systems such as boron nitride or transition metal dichalogenides, are also readily accessible using in situ biasing XPS.

■ ASSOCIATED CONTENT

Supporting Information

The Supporting Information is available free of charge on the ACS Publications website at DOI: 10.1021/acs.jpclett.6b01806.

Description of the sample preparation methodologies adopted, experimental details for the electrical characterization methods and for the biased-XPS instrumentation, and complete set of XPS spectra measured at different biases (PDF)

Energy band diagrams under flatband, accumulation, and depletion biasing conditions (PDF)

■ AUTHOR INFORMATION

Corresponding Author

*E-mail: rangan@physics.rutgers.edu. Phone: +1-848-445-8419.

Notes

The authors declare no competing financial interest.

■ ACKNOWLEDGMENTS

The authors thank Prof. Sefik Suzer and Dr. Hagai Cohen for their useful comments.

■ REFERENCES

(1) Lau, W. Use of surface charging in x-ray photoelectron spectroscopic studies of ultrathin dielectric films on semiconductors. *Appl. Phys. Lett.* **1989**, *54*, 338−340.

(2) Lau, W. A surface charging technique in photoemission spectroscopic studies of dielectric-semiconductor structures. *J. Appl. Phys.* **1990**, *67*, 1504−1509.

(3) Kwok, R.; Lau, W.; Landheer, D.; Ingrey, S. Surface charge spectroscopy: A novel surface science technique for measuring surface state distributions on semiconductors. *J. Electron. Mater.* **1993**, *22*, 1141−1146.

(4) Kwok, R.; Lau, W. Surface charge spectroscopy and its applications. *Prog. Surf. Sci.* **1995**, *50*, 357−376.

(5) Chan, R.; Kwok, R.; Lau, W. Modified surface charge spectroscopy for the characterization of insulator/semiconductor structures. *J. Appl. Phys.* **1996**, *79*, 3635−3639.

(6) Chan, R.; Kwok, R.; Lau, W.; Yan, H.; Wong, S. Studies of electrical and chemical properties of SiO2/Si after rapid thermal nitridation using surface charge spectroscopy and x-ray photoelectron spectroscopy. *J. Vac. Sci. Technol., A* **1997**, *15*, 2787−2792.

(7) Doron-Mor, I.; Hatzor, A.; Vaskevich, A.; van der Boom-Moav, T.; Shanzer, A.; Rubinstein, I.; Cohen, H. Controlled surface charging as a depth-profiling probe for mesoscopic layers. *Nature* **2000**, *406*, 382−385.

(8) Rozenblat, A.; Rosenwaks, Y.; Segev, L.; Cohen, H. Electrical depth profiling in thin SiON layers. *Appl. Phys. Lett.* **2009**, *94*, 053116.

(9) Rozenblat, A.; Rosenwaks, Y.; Cohen, H. Hot-electron characteristics in chemically resolved electrical measurements of thin silica and SiON layers. *Appl. Phys. Lett.* **2009**, *94*, 213501.

(10) Givon, A.; Piao, H.; McMahon, J.; Zorn, G.; Cohen, H. Contactless derivation of inner fields in gate-oxide layers: SiO2 on SiC. *Appl. Phys. Lett.* **2015**, *107*, 173101.

(11) Suzer, S. Differential charging in X-ray photoelectron spectroscopy: A nuisance or a useful tool? *Anal. Chem.* **2003**, *75*, 7026−7029.

(12) Ulgut, B.; Suzer, S. XPS studies of SiO_2/Si system under external bias. *J. Phys. Chem. B* **2003**, *107*, 2939−2943.

(13) Karadas, F.; Ertas, G.; Suzer, S. Differential charging in SiO2/Si system as determined by XPS. *J. Phys. Chem. B* **2004**, *108*, 1515−1518.

(14) Tasci, T. O.; Atalar, E.; Demirok, U. K.; Suzer, S. Electrical circuit modeling of surface structures for X-ray photoelectron spectroscopic measurements. *Surf. Sci.* **2008**, *602*, 365−368.

DOI: 10.1021/acs.jpclett.6b01806
J. Phys. Chem. Lett. 2016, 7, 3434−3439

(15) Suzer, S.; Sezen, H.; Ertas, G.; Dâna, A. XPS measurements for probing dynamics of charging. *J. Electron Spectrosc. Relat. Phenom.* **2010**, *176*, 52−57.
(16) Copuroglu, M.; Sezen, H.; Opila, R. L.; Suzer, S. Band-bending at buried SiO2/Si interface as probed by XPS. *ACS Appl. Mater. Interfaces* **2013**, *5*, 5875−5881.
(17) Copuroglu, M.; Aydogan, P.; Polat, E. O.; Kocabas, C.; Süzer, S. Gate-Tunable Photoemission from Graphene Transistors. *Nano Lett.* **2014**, *14*, 2837−2842.
(18) Aydogan, P.; Arslan, E.; Cakmakyapan, S.; Ozbay, E.; Strupinski, W.; Suzer, S. Voltage contrast X-ray photoelectron spectroscopy reveals graphene-substrate interaction in graphene devices fabricated on the C-and Si-faces of SiC. *Appl. Phys. Lett.* **2015**, *107*, 121603.
(19) Caliskan, D.; Sezen, H.; Ozbay, E.; Suzer, S. Chemical Visualization of a GaN pn junction by XPS. *Sci. Rep.* **2015**, *5*, 14091.
(20) Kobayashi, H.; Mori, T.; Namba, K.; Nakato, Y. New method for determination of energy distribution of surface states in the semiconductor band-gap: XPS measurements under biases. *Solid State Commun.* **1994**, *92*, 249−254.
(21) Kobayashi, H.; Yamashita, Y.; Mori, T.; Nakato, Y.; Komeda, T.; Nishioka, Y. Interface states for Si-based MOS devices with an ultrathin oxide layer: X-ray photoelectron spectroscopic measurements under biases. *Jpn. J. Appl. Phys.* **1995**, *34*, 959−964.
(22) Kobayashi, H.; Asano, A.; Asada, S.; Kubota, T.; Yamashita, Y.; Yoneda, K.; Todokoro, Y. Studies on interface states at ultrathin SiO2/Si (100) interfaces by means of x-ray photoelectron spectroscopy under biases and their passivation by cyanide treatment. *J. Appl. Phys.* **1998**, *83*, 2098−2103.
(23) Grunthaner, F.; Lewis, B.; Zamini, N.; Maserjian, J.; Madhukar, A. XPS studies of structure-induced radiation effects at the Si/SiO2 interface. *IEEE Trans. Nucl. Sci.* **1980**, *27*, 1640−1646.
(24) Lichterman, M. F.; Hu, S.; Richter, M. H.; Crumlin, E. J.; Axnanda, S.; Favaro, M.; Drisdell, W.; Hussain, Z.; Mayer, T.; Brunschwig, B. S.; et al. Direct observation of the energetics at a semiconductor/liquid junction by operando X-ray photoelectron spectroscopy. *Energy Environ. Sci.* **2015**, *8*, 2409−2416.
(25) Bersch, E.; Rangan, S.; Bartynski, R. A.; Garfunkel, E.; Vescovo, E. Band offsets of ultrathin high-κ oxide films with Si. *Phys. Rev. B: Condens. Matter Mater. Phys.* **2008**, *78*, 085114.
(26) Yan, R.; Zhang, Q.; Li, W.; Calizo, I.; Shen, T.; Richter, C. A.; Hight-Walker, A. R.; Liang, X.; Seabaugh, A.; Jena, D.; et al. Determination of graphene work function and graphene-insulator-semiconductor band alignment by internal photoemission spectroscopy. *Appl. Phys. Lett.* **2012**, *101*, 022105.
(27) Hollinger, G.; Himpsel, F. Probing the transition layer at the SiO2-Si interface using core level photoemission. *Appl. Phys. Lett.* **1984**, *44*, 93−95.
(28) Lau, W. Effects of a depth-dependent specimen potential on x-ray photoelectron spectroscopic data. *J. Appl. Phys.* **1989**, *65*, 2047−2052.
(29) Ogama, T. A new method to detect energy band-bending using x-ray photoemission spectroscopy. *J. Appl. Phys.* **1988**, *64*, 753−757.
(30) Schlaf, R.; Hinogami, R.; Fujitani, M.; Yae, S.; Nakato, Y. Fermi level pinning on HF etched silicon surfaces investigated by photoelectron spectroscopy. *J. Vac. Sci. Technol., A* **1999**, *17*, 164−169.
(31) Nishizawa, M.; Bolotov, L.; Kanayama, T. Simultaneous measurement of potential and dopant atom distributions on wet-prepared Si (111): H surfaces by scanning tunneling microscopy. *Appl. Phys. Lett.* **2007**, *90*, 122118.
(32) Hirayama, M.; Nakamura, J.; Natori, A. Band-bending effects on scanning tunneling microscope images of subsurface dopants: First-principles calculations. *J. Appl. Phys.* **2009**, *105*, 083720.
(33) Bom, N. M.; Soares, G. V.; de Oliveira Junior, M. H.; Lopes, J. M. J.; Riechert, H.; Radtke, C. Water Incorporation in Graphene Transferred onto SiO_2/Si Investigated by Isotopic Labeling. *J. Phys. Chem. C* **2016**, *120*, 201−206.
(34) Moser, J.; Verdaguer, A.; Jiménez, D.; Barreiro, A.; Bachtold, A. The environment of graphene probed by electrostatic force microscopy. *Appl. Phys. Lett.* **2008**, *92*, 123507.
(35) Ni, Z. H.; Wang, H. M.; Luo, Z. Q.; Wang, Y. Y.; Yu, T.; Wu, Y. H.; Shen, Z. X. The effect of vacuum annealing on graphene. *J. Raman Spectrosc.* **2010**, *41*, 479−483.
(36) Giusca, C. E.; Panchal, V.; Munz, M.; Wheeler, V. D.; Nyakiti, L. O.; Myers-Ward, R. L.; Gaskill, D. K.; Kazakova, O. Water Affinity to Epitaxial Graphene: The Impact of Layer Thickness. *Adv. Mater. Interfaces* **2015**, *2*, 1500252.

DOI: 10.1021/acs.jpclett.6b01806
J. Phys. Chem. Lett. 2016, 7, 3434−3439